



Design and Development of High Sensitive Surface Plasmon Resonance Biosensors for Glucose Detection

Kazi Mustafizur Rahman¹ · Faysal Nayan¹ · Raihan Ahmed¹ · Mushfiquur Rahman¹

Received: 8 June 2024 / Accepted: 29 July 2024

© The Author(s), under exclusive licence to Springer Science+Business Media, LLC, part of Springer Nature 2024

Abstract

This paper presents a surface plasmon resonance (SPR) sensor utilizing a prism-coupled Ag/ZnSe/BP hybrid structure with improved sensitivity for glucose detection in urine samples. In this Kretschmann configuration, multilayers are vertically stacked together to improve the optical and electronic properties of the proposed SPR sensor. The transfer matrix method (TMM) is used for the theoretical model and to analyze the performance of the sensors. The proposed SPR sensor comprises 2D materials such as black phosphorus (BP), which improve the sensitivity of the SPR-based sensor through efficient interactions with biomolecules. The resonance angle of surface plasmons shifts due to a difference in the refractive index from 1.330 to 1.337 in urine samples with various glucose levels. Initially, the study aims to compare the sensor performance parameters among different prisms (CaF₂, BK7, FK51A, and SF10) coupled with a hybrid structure. The proposed sensor achieved a noticeably higher value sensitivity of 511 (deg./RIU), a quality factor of 108.377 (1/RIU), and a figure of merit of 108.374 when a CaF₂ prism with an optimized thickness was used. The performance parameters, including the sensitivity, full width at half maximum (FWHM), figure of merit (FoM), and detection accuracy (DA), were measured, and the results were compared to evaluate the findings. The proposed structure can be more effective in detecting different liquid analytes in biosensing applications, including glucose detection.

Keywords Biosensor · Black phosphorus · Glucose concentration detection · Optimized performance · Surface plasmon resonance · Transfer matrix method

Introduction

During the last decade, surface plasmon resonance (SPR) sensing devices have undergone considerable development [1, 2], both from the fundamental point of view and from the design of highly sensitive devices for optical sensing of small chemical or biological entities [3].

Kretschmann [4] and Otto [5, 6] are the available configurations for SPR sensors. The prism surface is coated with a metal film in the Kretschmann configuration, whereas an air gap is maintained between the prism and the metal interface in the Otto configuration. Light bounces directly from the prism to the metal film in the Kretschmann configuration, and this property makes the Kretschmann configuration

more popular than the Otto configuration [7]. Optical sensors offer novel features, such as high sensitivity, quantitative response, rapid detection, and selectivity.

Ag layered sensors are less expensive than are Au layered sensors. Moreover, Ag maintains higher detection accuracy (DA) by offering a sharper dip in the resonance curve and keeping the full-width half maximum (FWHM) narrower [8]. ZnSe is a well-known semiconductor material used in optoelectronic research, fabrication of laser diodes, field emitters, photodetectors, solar cells, photocatalysis, in vivo imaging, and sensors [9]. Here, a zinc selenide (ZnSe) layer is used to protect the silver (Ag) layer from oxidation and to increase the sensitivity. The combination of zinc selenide and silver was studied in detail in [10].

A high surface-to-volume ratio, greater biomolecule absorption, high mobility, high charge density, direct band gap, and better binding to various molecules promote the use of 2D black phosphorus (BP) thin films in biosensors [11]. In addition, BP is an excellent choice for chemical applications with high-performance potential because it

✉ Kazi Mustafizur Rahman
abeer1147715753@gmail.com

¹ Department of Electrical and Electronic Engineering,
Ahsanullah University of Science and Technology, Dhaka,
Bangladesh

exhibits appealing chemical, physical, and mechanical anisotropic properties [12]. For example, the implementation of a bilayer of BP over a conventional gaseous sensor enhances its sensitivity by 35%, and Srivastava et al. reported this fact numerically [13].

SPR-based sensors are useful in the fields of food safety [14], environmental monitoring [15], and biomedicine [16]. Recently, SPR sensors have been used to detect blood plasma concentrations [17], fat concentrations in milk [18], basal cancer cells [19], infected red blood cells (IRBCs) [20], and blood sugar levels [21]. To carry out the metabolic processes necessary for existence, energy is needed by every human cell. Glucose is an important source of energy for human cells. Unfortunately, excessive glucose intake may result in diabetes, a chronic metabolic disease. Therefore, a balanced diet of glucose should be maintained to prevent damage to the kidneys, eyes, heart, nervous system, and other organs [22]. According to a World Health Organization (WHO) report, more than 1.6 million people have died, and approximately 422 million people have been affected globally [23].

In urine, increased glucose concentrations cause renal glycosuria [24]. The levels of several body fluids and urine samples change with changes in glucose concentration. In the urine sample, the refractive index varies with the change in glucose concentration of the affected person from the average healthy person. Normally, the human body does not have glucose in the range of 0–15 mg/dL [25]. The unit of glucose concentration is expressed in mg per deciliter (mg/dL). Typically, the range of 0–15 mg/dL glucose concentration in the human body is absent. It is essential to supply energy to our tissues and cells and maintain optimal blood sugar levels to prevent hypoglycemia (low blood sugar) and hyperglycemia (high blood sugar). Renal glycosuria generally increases as glucose levels increase in urine samples (in the range of 165 to 180 mg/dL). Hypoglycemia indicates that the glucose concentration is less than 40 mg/dL, and hyperglycemia indicates that the glucose concentration is between 279 and 360 mg/dL [25].

The research work is divided into distinct sections. First, the structures of the four different biosensors with the necessary theories are provided. Second, the models are analyzed via different plots and charts to determine the highest sensitivity and optimum conditions at the operating wavelength of 633 nm. Third, an evaluation is developed by varying the thickness of the layers for the designed structure. Additionally, the proposed sensor characteristics and fabrication process are presented. Fourth, the results under a variety of scenarios are carried out for the detection of glucose concentration, and the SPR biosensors are compared with previously reported SPR setups. Finally, the conclusion summarizes the key insights of the paper.

Methodology

In this section, design considerations and theories for the development of four biosensors are discussed.

A. Design of the Proposed SPR Sensor Device

The proposed SPR sensor setup is shown in Fig. 1. It is a five-layer structure in which the sensing medium (SM) has a reflectance of 1.33 to 1.337. Here, four types of prisms are used to design four structures. In these four structures, the layers are individually varied to obtain better performance. The wavelength is taken as 633 nm for all the configurations.

Here, the four structures are named Sensor-1, Sensor-2, Sensor-3, and Sensor-4. Sensor-1 is structured as CaF₂/Ag/ZnSe/BP/SM, sensor-2 is structured as BK7/Ag/ZnSe/BP/SM, sensor-3 is structured as FK51A/Ag/ZnSe/BP/SM, and sensor-4 is structured as SF10/Ag/ZnSe/BP/SM. The optimum thicknesses of the materials in the four different configurations are listed in Table 1. The thicknesses of different layers of the designed biosensors were determined by analyzing recent research on biosensors. In addition, for these thicknesses, high sensitivity and optimum results were found and checked. Moreover, for other thickness

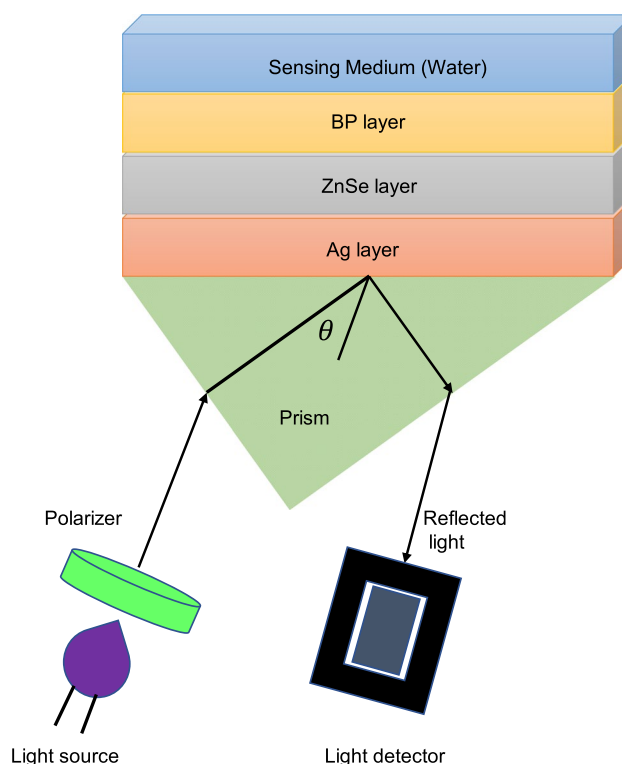


Fig. 1 Schematic diagram of the proposed five-layered SPR biosensor (Prism/Ag/ZnSe/BP/SM-based) for the determination of glucose levels

Table 1 Optimized thickness of the materials for different prisms used to design biosensors

Sensor No.	Prism used	Ag thickness	ZnSe thickness	BP thickness
1	CaF2	46	2	1
2	BK7	50	9	1
3	FK51A	56	3	3
4	SF10	48	10	6

Table 2 Refractive indices of the materials

Layer number	Layer material	Refractive index	Reference
1a	CaF2	1.4329	[26, 27]
1b	BK7	1.515	[16, 28]
1c	FK51A	1.4853	[29]
1d	SF10	1.7231	[30, 31]
2	Ag	0.06656 + 4.0452i	[31, 32]
3	ZnSe	2.578	[31, 33]
4	BP	3.5 + 0.01i	[34, 35]
5	Water	1.330 to 1.337	[7, 27]

combinations, the reflectance curves were not smooth, the SPR curves obtained were flat (no significant dip), provided unexpected values, and may have resulted in practically unsuitable conditions.

Many recent studies have analyzed the design of SPR biosensors with high sensitivity and optimal results. The refractive indices (RIs) for all the materials used in this study are listed in Table 2.

B. Mathematical Expressions

The proposed sensors are designed on the basis of the Kretschmann configuration [4]. In this SPR setup, the plasmonic wave moves along the interface between the sensing medium and the metallic layer when the light beam resonantly impacts the metallic layer through the prism at a specific angle. Here, the resonance condition is described by the waveforms that satisfy the condition that the wavevector of the incident p-polarized light equals the surface plasmon wave. The mathematical expression for the matching condition is [36].

$$K_x = K_{sp} \tag{1}$$

where K_x and K_{sp} are the wave vectors of the incident light and the surface plasmon wave (SPW) vectors, respectively. These are defined by [36]

$$K_x = \frac{2\pi}{\lambda} n_p \times \sin\theta_0 \tag{2}$$

$$K_{sp} = \frac{2\pi}{\lambda} \times \sqrt{\frac{\epsilon_1 \times \epsilon_2}{\epsilon_1 + \epsilon_2}} \tag{3}$$

where n_p is the RI of the prism, λ is the wavelength of the incident light, θ_0 is the light incidence angle at the interface between the prism and the metal layer, and ϵ_1, ϵ_2 are the dielectric constants of the sensing medium and the metal layer, respectively.

With a change in the refractive index, the SPW propagation constant also changes directly. Therefore, the incident angle must be satisfied to meet the equality conditions given in Eq. (1). The energy of the incident light is transferred completely to the SPW with minimum reflectivity at the resonance state. The SPR sensor is intended to detect the angle at resonance (minimum reflectivity), and any change in this angle means a change in the refractive index.

One of the best methods for characterizing reflectivity is the transfer matrix method (TMM). It is a precise approach because there are no approximations in this method [37].

The transmittance and reflectance calculations for the multilayer model are performed by assuming that the layers are thinly homogeneous and stacked on each other. Additionally, it is assumed that each layer is uniform, symmetric, and nonmagnetic [38].

The reflectance of incident p-polarized light is defined as [23]

$$R_p = |r_p|^2 \tag{4}$$

where r_p is the amplitude of the reflected wave that can be calculated for the N -layer model from [23]

$$r_p = \frac{(F_{11} + F_{12}q_N)q_1 - (F_{21} + F_{22}q_N)}{(F_{11} + F_{12}q_N)q_1 + (F_{21} + F_{22}q_N)} \tag{5}$$

According to the transfer matrix method, the wave propagation parameters for the N -layer model that describes the light propagation from layer (N) to layer ($N + 1$) can be calculated through the F_{ij} matrix, [23]

$$F_{ij} = \left[\prod_{k=2}^{N-1} \begin{pmatrix} \cos\beta_k & \frac{-i\sin\beta_k}{q_k} \\ -iq_k\sin\beta_k & \cos\beta_k \end{pmatrix} \right] \tag{6}$$

$$F_{ij} = \begin{bmatrix} F_{11} & F_{12} \\ F_{21} & F_{22} \end{bmatrix} \tag{7}$$

where β_k is the random phase constant and q_k is the admittance at the k th layer, calculated by [39]

Fig. 2 The reflectance curve plot of Sensor-1 (CaF₂/Ag/ZnSe/BP/SM) at different RIs (1.330–1.337)

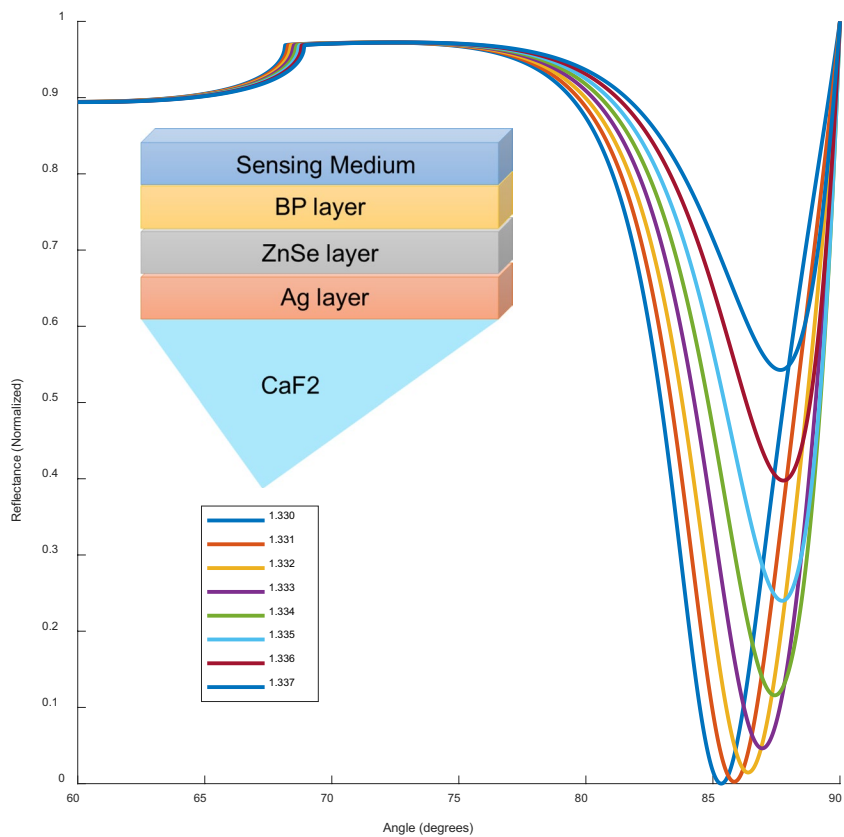


Fig. 3 Reflectance curve plot of Sensor-2 (BK7/Ag/ZnSe/BP/SM) at different RIs (1.330–1.337)

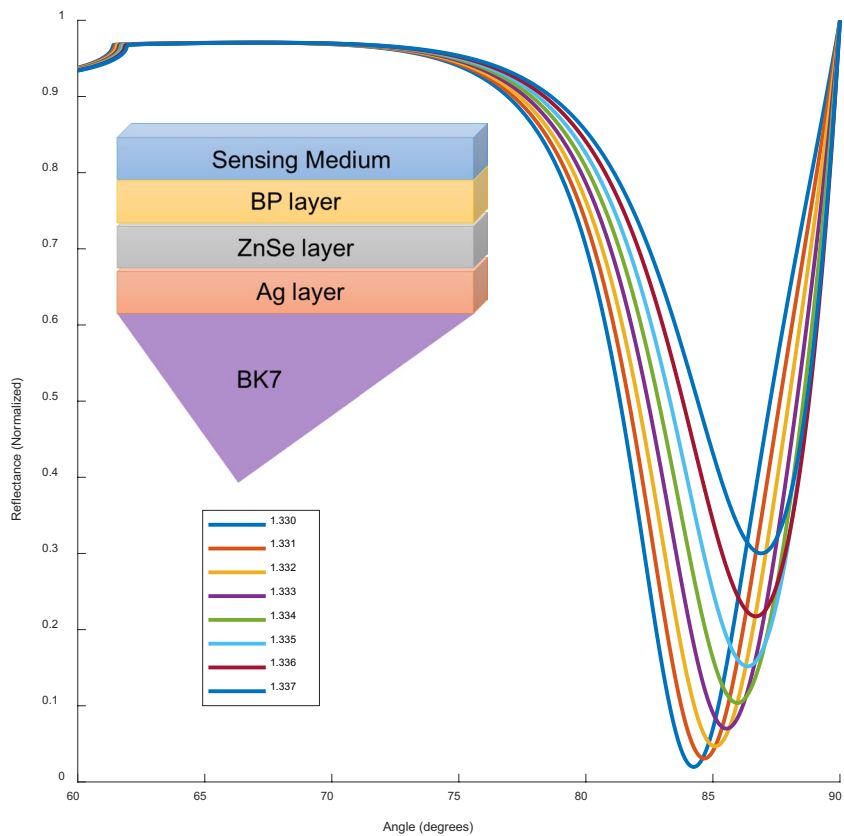


Fig. 4 Reflectance curve plot of Sensor-3 (FK51A/Ag/ZnSe/BP/SM) at different RIs (1.330–1.337)

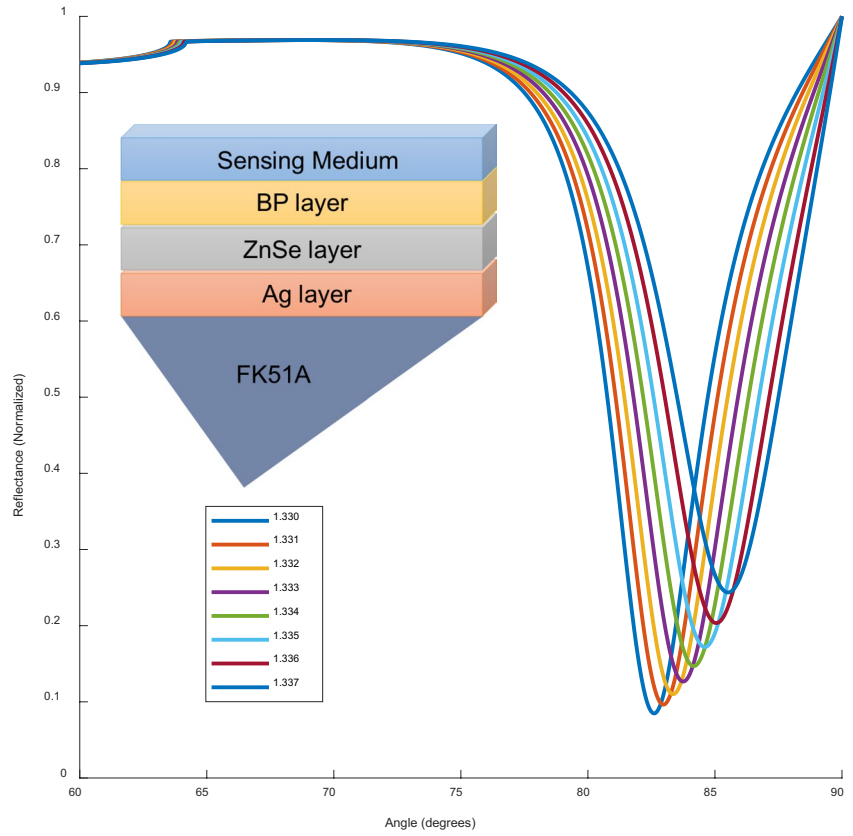


Fig. 5 Reflectance curve plot of Sensor-4 (SF10/Ag/ZnSe/BP/SM) at different RIs (1.330–1.337)

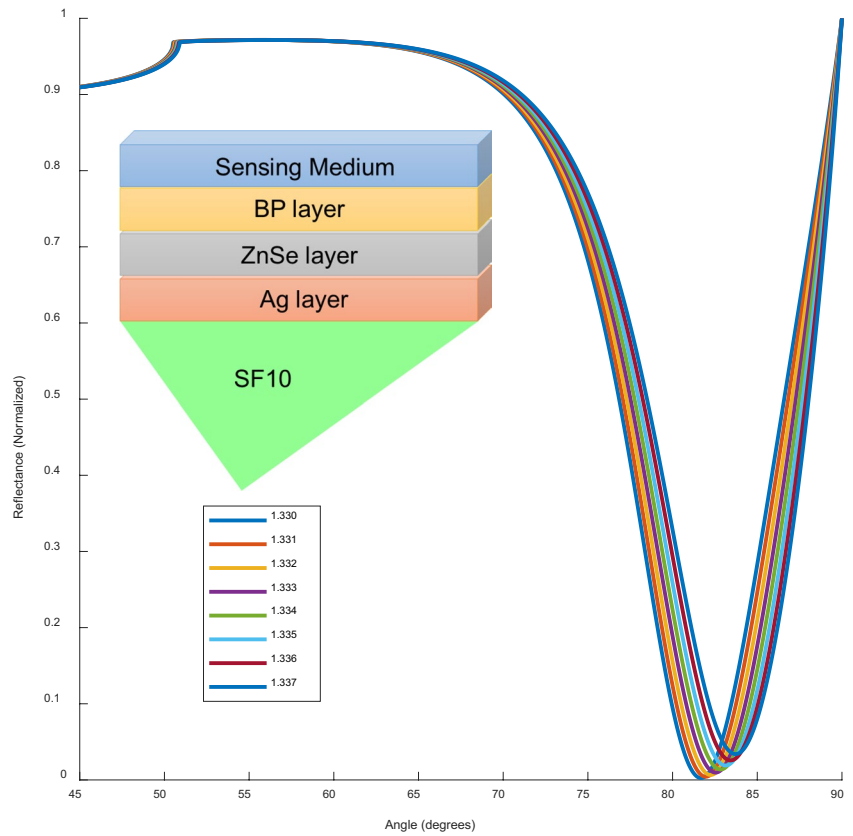
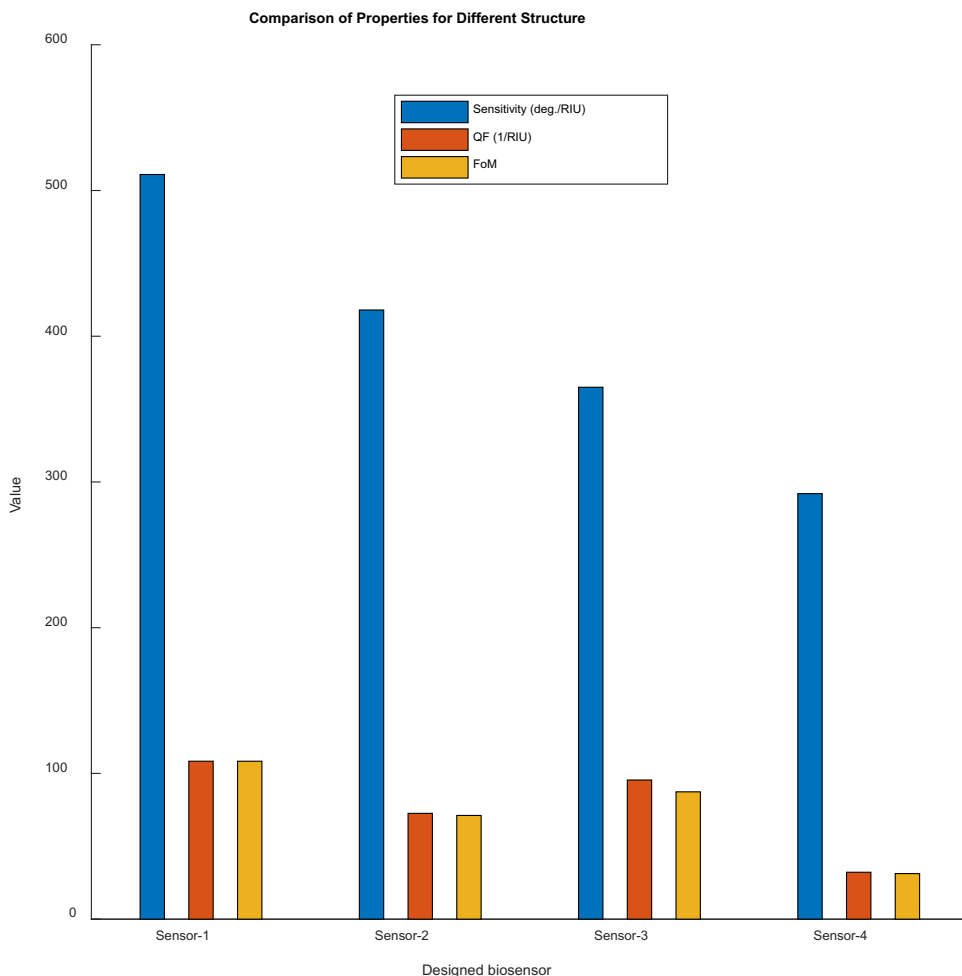


Table 3 Performance parameters of the biosensors (Sensor-1, Sensor-2, Sensor-3, and Sensor-4)

Sl No.	S	QF	FoM	FWHM	Angle shift	DA
1	511	108.377	108.374	4.715	0.503	0.2120
2	418	72.594	71.166	5.758	0.432	0.1736
3	365	95.474	87.372	3.822	0.387	0.2615
4	292	32.183	31.264	9.072	0.191	0.1102

Fig. 6 Comparison of the sensitivity, QF, and FoM values for the designed SPR biosensors (Sensor-1, Sensor-2, Sensor-3, and Sensor-4) via a bar graph



$$\beta_k = \frac{2\pi}{\lambda} d_k \sqrt{n_k^2 - (n_p \sin\theta_0)^2} \tag{8}$$

$$q_k = \frac{\sqrt{n_k^2 - (n_p \sin\theta_0)^2}}{n_k^2} \tag{9}$$

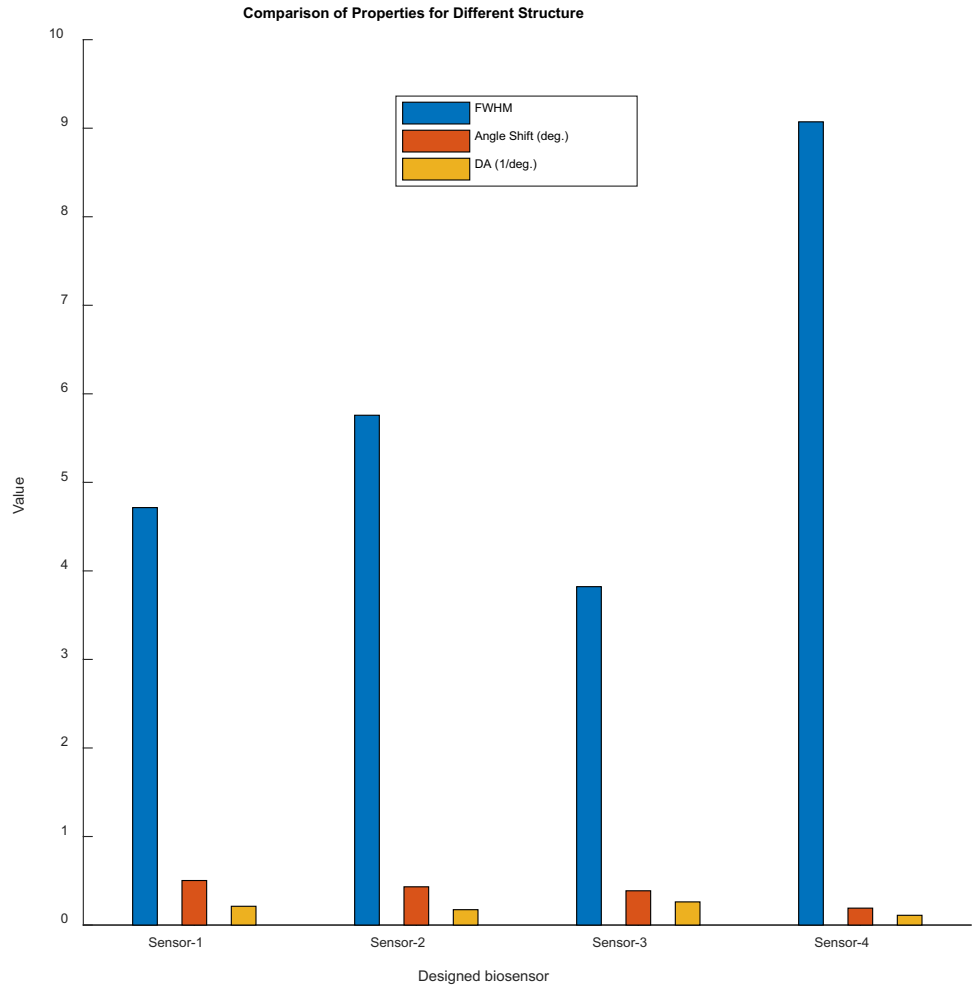
Here, n_p is the RI of the prism, and θ_0 is the incidence angle at the prism–metal interface. d_k is the thickness of the k th layer, and n_k is the reflective index.

C. Performance Parameters of the Sensor

The sensitivity (S) is defined as the ratio of the deviation in the SPR angle ($\Delta\theta_{res}$) and the deviation in the sensing medium’s RI (Δn) [40, 41]. The expression can be found in Eq. (10):

$$S = \frac{\Delta\theta_{res}}{\Delta n} (indeg/RIU) \tag{10}$$

Fig. 7 Comparison of the FWHM, angle shift, and DA values for the designed SPR biosensors (Sensor-1, Sensor-2, Sensor-3, and Sensor-4) via a bar graph



The detection accuracy (*DA*) is computed as the ratio of $\Delta\theta_{SPR}$ to the FWHM. The expression of the DA can be found in Eq. (11):

$$DA = \frac{1}{FWHM} (indeg^{-1}) \tag{11}$$

The full width at half maximum (FWHM) provides information about the width and sharpness of the reflectance curve. The expression for the FWHM can be found in Eq. (12):

$$FWHM = \theta_2 - \theta_1 (indeg) \tag{12}$$

Here, θ_2, θ_1 indicate the difference between the incidence angles at half (50%) of the reflectivity.

To ascertain the sensing efficiency, another scale is the figure of merit (FoM) scale. Finding the ideal mix of components, layout, and circumstances produces a high FoM, indicating great performance, sensitivity, and efficiency. The FoM can be expressed as shown in Eq. (13):

$$FoM = \frac{S(1 - R_{min})}{FWHM} \tag{13}$$

The quality factor (*QF*) provides information about the resolution of the proposed SPR sensor. The expression of QF can be found in Eq. (14):

$$QF = \frac{S}{FWHM} (inRIU^{-1}) \tag{14}$$

These parameters are optimized for all of the surface plasmon resonance biosensors designed in this study.

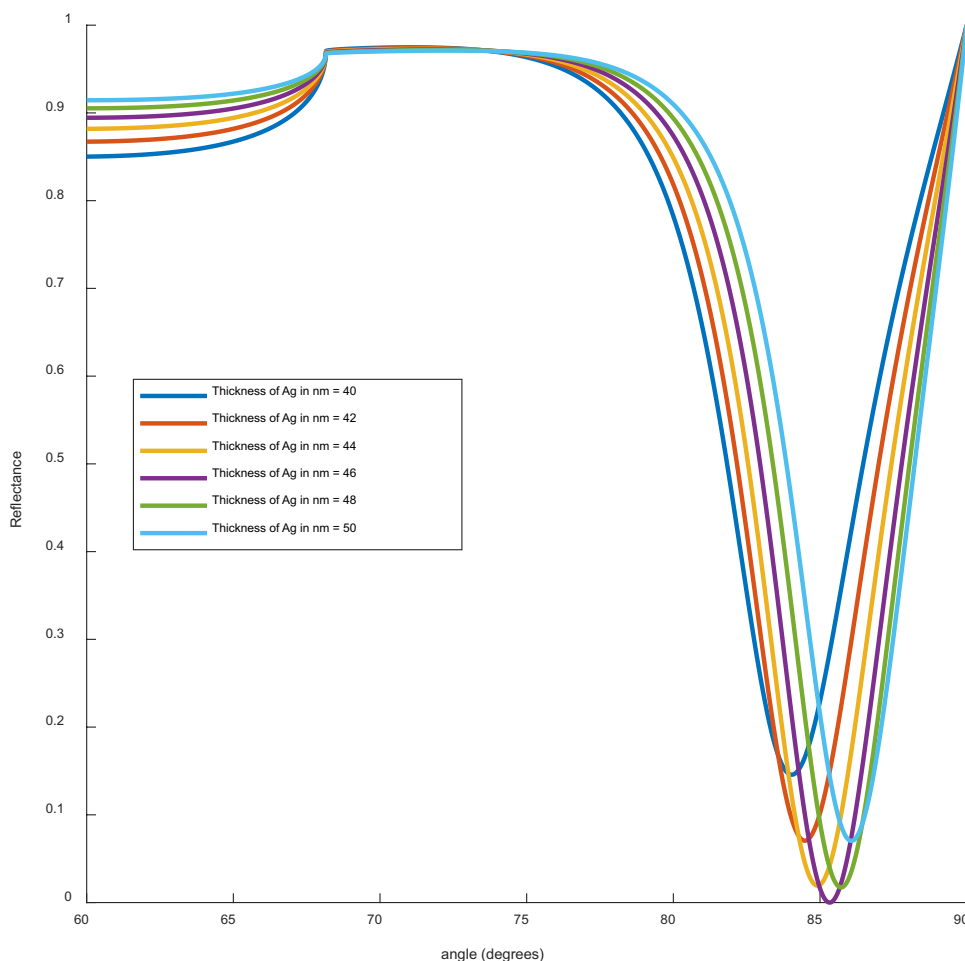
Results

This module can be divided into four sections:

A. Parameters for Optimized Thickness

The reflectance as a function of the angle of incidence plot for the four different biosensor structures (Sensor-1, Sensor-2, Sensor-3, and Sensor-4) is depicted in Figs. 2, 3, 4, and 5, respectively. Here, the SPR reflectance plots were

Fig. 8 Reflection intensity plot with thicknesses of $d_{Ag} = 40, 42, 44, 46, 48,$ and 50 nm; $d_{ZnSe} = 2$ nm; and $d_{BP} = 1$ nm



plotted for different RIs ranging from 1.33 to 1.337, with an RI change of 0.001.

The performance parameters obtained from the different sensors (Sensor-1, Sensor-2, Sensor-3, and Sensor-4) are tabulated in Table 3, and for easy recognition of the differences in the performance parameters, bar graphs are presented in Figs. 6 and 7. These results indicate that Sensor-1 has the highest sensitivity, with a sensitivity of 511 deg/RIU and an FoM of 108.374.

Here, the unit of sensitivity is deg/RIU, QF is 1/RIU, FWHM is deg, and DA is 1/deg. An analysis of the results confirmed that the combination of Sensor-1 (CaF₂/Ag/ZnSe/BP/SM) results in the highest sensitivity, a perfect dip in the reflectance curve, and optimum results.

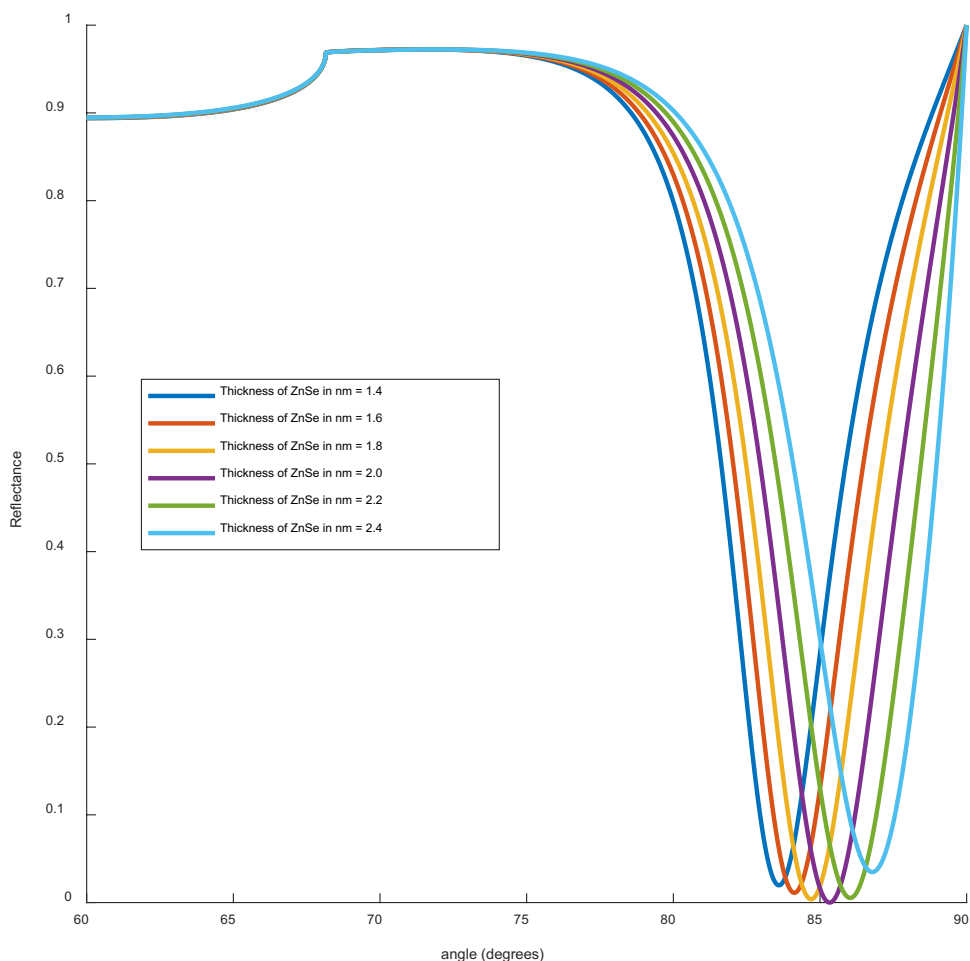
B. Thickness Optimization of the Layers for Sensor-1

Sensor-1 (CaF₂/Ag/ZnSe/BP/SM) shows better sensitivity and overall performance. Therefore, with water as the sensing medium, we examined the sensor performance at different material thicknesses.

Initially, taking water as a sensing medium, we optimized the thickness of the Ag layer with a fixed thickness of the ZnSe layer ($d_{ZnSe} = 2$ nm) and BP layer ($d_{BP} = 1$ nm). Figure 8, clearly shows that the reflection intensity depends on the thickness of the Ag layer, and the optimized thickness is 46 nm. Similarly, taking water as a sensing medium, the thickness of the ZnSe layer was optimized with a fixed thickness of the Ag layer ($d_{Ag} = 46$ nm) and BP layer ($d_{BP} = 1$ nm). Figure 9 clearly shows that the reflection intensity depends on the thickness of the ZnSe layer, and the optimized thickness is 2 nm.

Finally, with water as the sensing medium, we optimized the thickness of the BP layer to a fixed thickness of the Ag layer ($d_{Ag} = 46$ nm) and ZnSe layer ($d_{ZnSe} = 2$ nm). Figure 10 clearly shows that the reflection intensity depends on the thickness of the BP layer, and the optimized thickness is 1 nm. Using this comparative analysis, the thickness of the layers for all the sensors was selected. These plots help us choose the correct combination of materials with the optimum thickness for designing SPR biosensors.

Fig. 9 Reflection intensity plot with a thickness of $d_{Ag} = 46$ nm, $d_{ZnSe} = 1.4, 1.6, 1.8, 2.0, 2.2,$ and 2.4 nm, and $d_{BP} = 1$ nm



C. Analysis of Different Performance Parameters for Sensor-1 (CaF2 Prism)

For further analysis, we used Sensor-1 (CaF2/Ag/ZnSe/BP/SM) because it has better performance. For the characterization of Sensor-1, the thickness of Ag was varied to study the changes in other parameters. The thickness varied from 40 to 50 nm, and the variations in the sensitivity, FoM, and angle shift are listed in Table 4; a plot of these quantities is shown in Fig. 11.

A CaF2 glass prism/Ag/ZnSe/BP/SM nanostructure was utilized. The silver layer is employed in a variety of thicknesses between 40 and 50 nm, with steps of 1 nm. The sensitivities are calculated and found to be 393, 413, 433, 452, 473, 492, 511, 527, 540, 547, and 550 deg/RIU, corresponding to silver layer thicknesses of 40, 41, 42, 43, 44, 45, 46, 47, 48, 49 and 50 nm, respectively. The optimal thickness of the Ag layer is 46 nm, which will be considered in the next investigation.

Similarly, the influences of certain factors on the sensitivity of the SPR photosensor to the metal thickness, number of

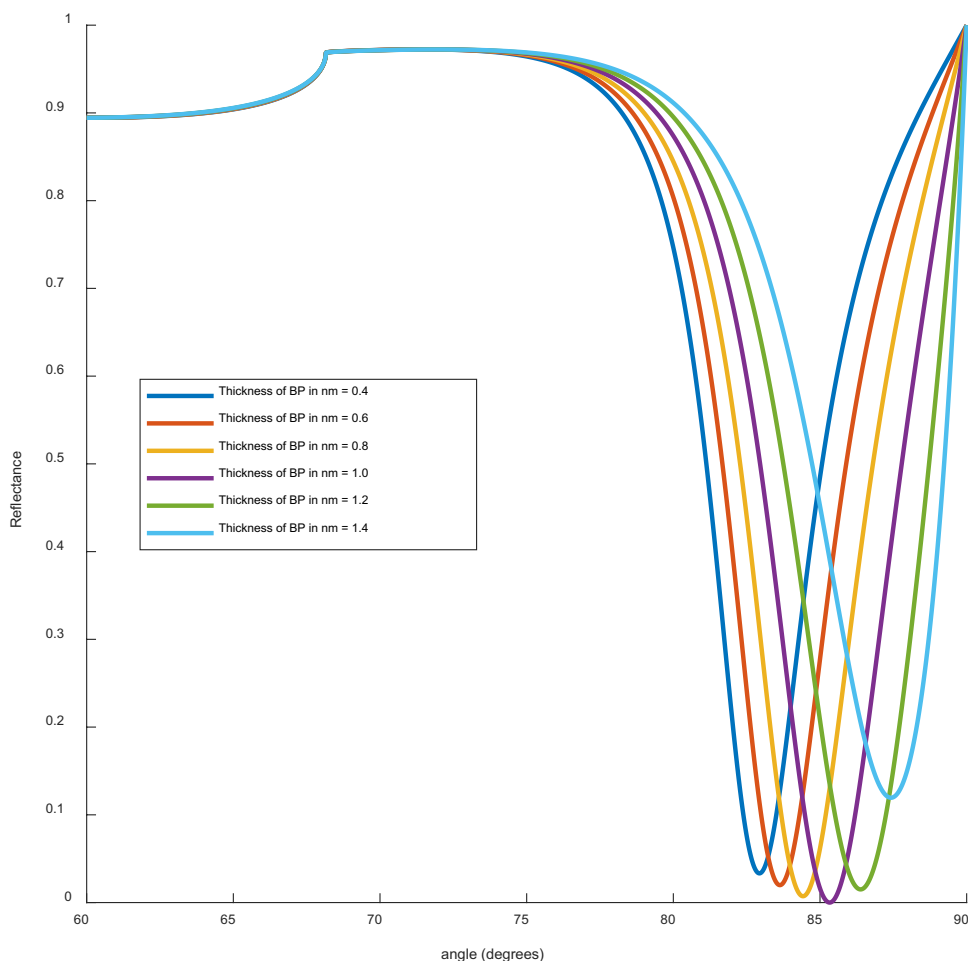
2D nanomaterial layers, and thickness of the ZnSe material are investigated. For all the sensors designed in this study, the BP and ZnSe layer thicknesses are varied between 1 and 10 nm, with steps of 1 nm. The thickness has been varied for all the designed structures, and the resonant dip in the reflectance spectra with optimized parameters is not available beyond these thicknesses.

The FWHM, DA, and QF are also calculated by varying the Ag thickness, as shown in Table 5. Further characterizations are performed by varying other parameters with increasing Ag thickness, as shown in Figs. 12 and 13. The results show that the QF and FOM have almost the same values because of the very low value of the minimum reflectance.

D. Mechanism of Glucose Detection in Urine Samples

Diabetism occurs due to the intake of an unbalanced diet, genetic reasons, and inactivity in performing physical activities. If a patient with diabetes has varying glucose levels

Fig. 10 Reflection intensity plot with thicknesses of $d_{Ag} = 46$ nm, $d_{ZnSe} = 2$ nm, and $d_{BP} = 0.4, 0.6, 0.8, 1.0, 1.2,$ and 1.4 nm



in their urine, the sensor can be used to detect changes by placing urine samples. This sensor increases the refractive index, which corresponds to higher glucose concentrations, by shifting the surface plasmon resonance (SPR) angle to the right.

Table 4 Values of sensitivity, FoM, and angle shift due to silver thickness variation

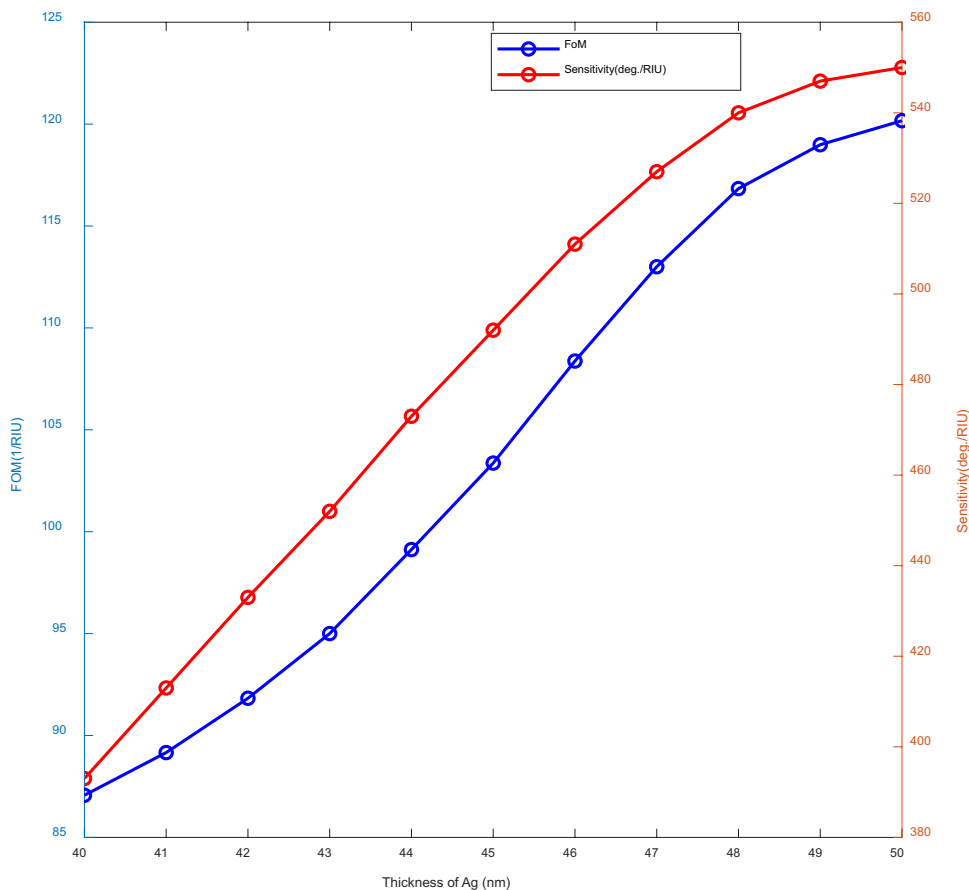
Sl. No.	Ag thickness	Sensitivity	FoM	Angle shift
1	40	393	87.06871	0.361
2	41	413	89.16228	0.441
3	42	433	91.82750	0.450
4	43	452	95.00195	0.454
5	44	473	99.12307	0.474
6	45	492	103.3678	0.488
7	46	511	108.3748	0.503
8	47	527	113.0014	0.527
9	48	540	116.8355	0.531
10	49	547	118.9894	0.554
11	50	550	120.1672	0.547

Here, as shown in Table 6, we collected urine samples with glucose concentrations of 0–15 mg/dL, 0.625 gm/dL, and 1.25 gm/dL, with refractive indices of 1.335, 1.336, and 1.337, respectively [42]. Similarly, samples at lower glucose concentrations were measured, and the corresponding refractive indices ranged from 1.330 to 1.334.

For an RI change of 0.001, the maximum sensitivity is 511 deg/RIU, and a minimum reflectance of 0.000024 is observed. For glucose concentration variation from 0–15 mg/dL to 0.625 gm/dL, the angle of incidence shifts to 87.78 degrees from 87.83 degrees for 0.001 RI variation. Thus, two urine samples were tested with the proposed bio-sensor: a normal human urine sample (0~15 mg/dL) with an RI of 1.335, which is a reference value, and a higher glucose level (0.625 gm/dL) with an RI of 1.336. For a 0.001 increment in the RI, the minimum SPR angle difference ($\Delta \theta_{SPR}$) becomes 0.05 degrees, and the minimum reflectance also increases to 0.3976.

Furthermore, for the sample variation from 0.625 gm/dL to 1.25 gm/dL, we obtain a refractive index variation of 0.001, and the SPR angle shift is from 87.78 to 87.66. Hence, when the concentration of glucose is changed from

Fig. 11 Variation in FoM (figure of merit) and sensitivity (S) as a function of Ag thickness for Sensor-1 (CaF₂/Ag/ZnSe/BP/SM)



0.625 gm/dL gm/dL, a reference value, to 1.25 gm/dL, *R_{min}* increases from 0.3976 to 0.5427. Additionally, the $\Delta \theta_{SPR}$ increases to 0.12 degrees.

The output detector measures this shift in the SPR angle, enabling the accurate detection of glucose levels in the urine samples. A comparison with earlier research is listed in Table 7.

Table 5 FWHM, DA, and QF values due to silver thickness variations in the surface plasmon resonance biosensor

Sl. No.	Ag thickness	FWHM	DA	QF
1	40	4.513	0.22158	87.08176
2	41	4.632	0.21588	89.16234
3	42	4.714	0.21213	91.85405
4	43	4.756	0.21026	95.03784
5	44	4.768	0.20973	99.20302
6	45	4.757	0.21021	103.4265
7	46	4.715	0.21208	108.3775
8	47	4.645	0.21528	113.4553
9	48	4.542	0.22016	118.8903
10	49	4.415	0.22650	123.8958
11	50	4.225	0.23501	129.2596

Fabrication

The fabrication process is explained in Fig. 14. The fabrication of Ag, ZnSe, and BP layers, which are utilized to make SPR chips, was first performed. A solution containing acetone vapor, methanol, and deionized water was applied to the glass prism. A thermal evaporator system performs physical vapor deposition (PVD) of metal layers on prism glass [49]. The BP layer can be made via a well-known chemical vapor deposition (CVD) procedure [50], which can then be chemically transferred over a ZnSe layer. After being manufactured, these chips are placed on top of the prism.

A urine sample is subsequently poured onto the sensor chip area for sensing purposes. Finally, the complete SPR chip is set over a spinning table. The reflected light is received by an optical detector on the output side of the prism, which measures its intensity.

Conclusion

This paper introduces and examines four novel, high-sensitivity, low-cost SPR biosensors for detecting glucose. The transfer matrix method (TMM) and Fresnel’s equations are applied to analyze the reflectance spectra. The

Fig. 12 FWHM (full width at half maximum) and DA (detection accuracy) are plotted as a function of Ag thickness for Sensor-1 (CaF₂/Ag/ZnSe/BP/SM)

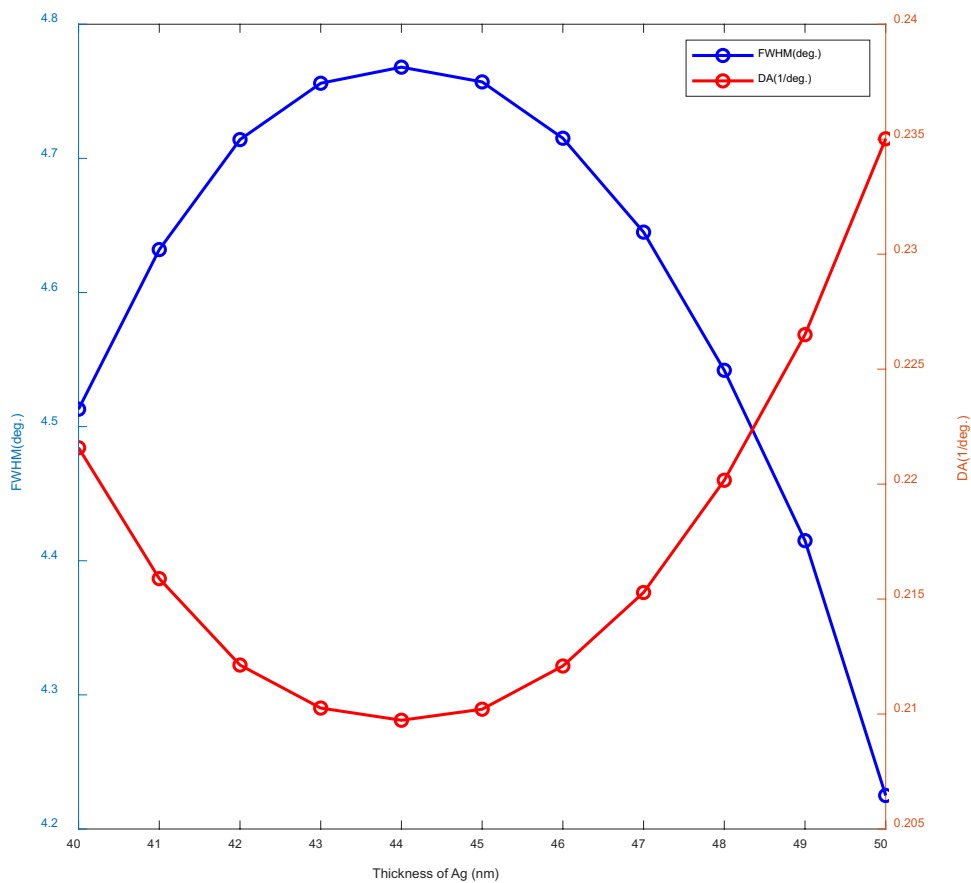


Fig. 13 Variation in the SPR angle shift and sensitivity for different Ag thicknesses for Sensor-1

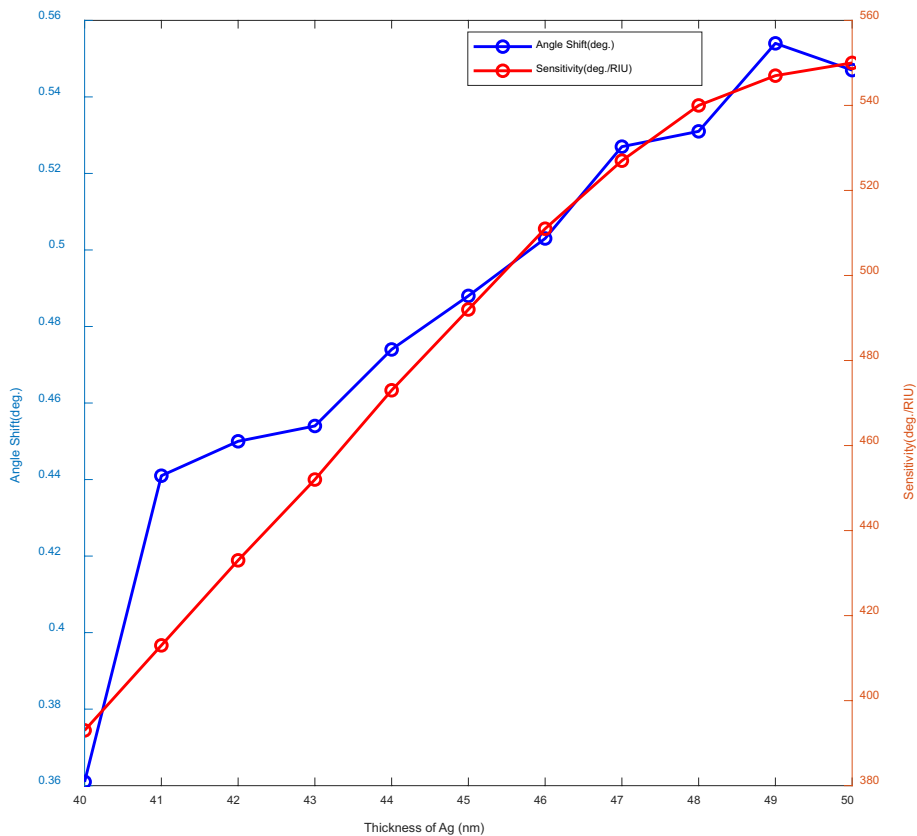


Table 6 Glucose level detection in urine samples via Sensor-1

Glucose level	Ref. index	θ_{SPR}	$\Delta \theta_{SPR}$	R_{min}
0–15 mg/dL	1.330	85.336	Ref	0.000024
	1.331	85.839	0.503	0.002491
	1.332	86.38	0.541	0.01459
	1.333	86.94	0.56	0.04628
	1.334	87.44	0.5	0.1159
1.335	87.83	0.39	0.2399	
0.625 gm/dL	1.336	87.78	0.05	0.3976
1.25 gm/dL	1.337	87.66	0.12	0.5427

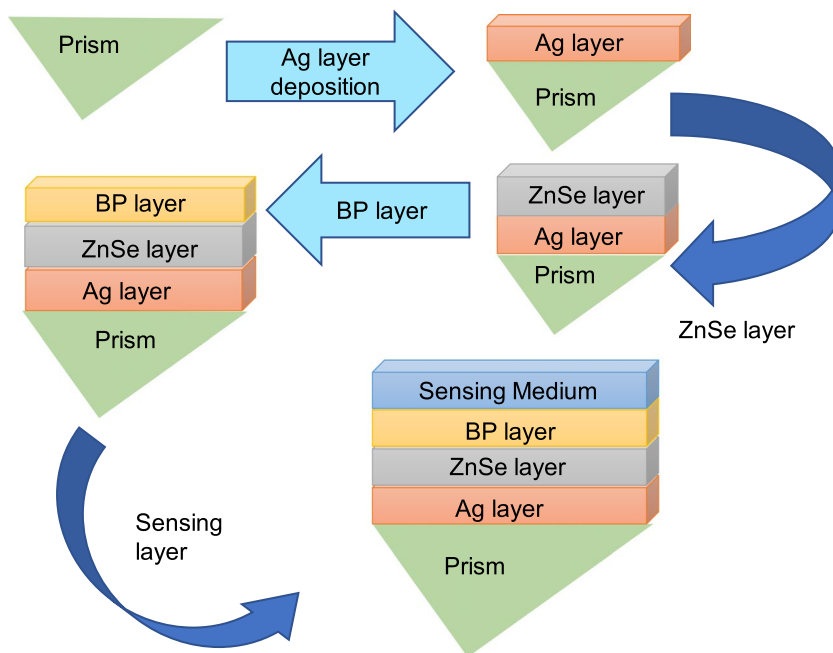
Table 7 Comparison of the proposed biosensor with other existing biosensors

Structures of models	S	QF	References
Prism/Ag/MXene/ZnO/Graphene	136.5	38.7	[43]
Prism/ZnO/Ag/Au/BaTiO3/Graphene	116.67	37.87	[44]
Gold/SnSe/Gold/Graphene/SM	327.6	-	[35]
Prism/Ag/MXene/SM	212.54	-	[45]
Prism/ZnO/Au/MoS2/graphene	101.58	15.11	[46]
Prism/Ag/barium titanate/graphene/SM	300	83.102	[47]
N-FK51A prism/Ag/Si/BP/SM	322.66	-	[48]
CaF2/Ag/ZnSe/BP/SM	511	108.377	Present Work
BK/Ag/ZnSe/BP/SM	418	72.594	Present Work
FK51A/Ag/ZnSe/BP/SM	365	95.474	Present Work
SF10/Ag/ZnSe/BP/SM	292	32.183	Present Work

optimized configurations for sensors 1 to 4 consisted of five layers: CaF2/Ag(46 nm)/ZnSe(2 nm)/BP(1 nm)/sensing medium, BK7/Ag(50 nm)/ZnSe(9 nm)/BP(1 nm)/sensing medium, FK51A/Ag(56 nm)/ZnSe(3 nm)/BP(3 nm)/sensing medium, and SF10/Ag(48 nm)/ZnSe(10 nm)/BP(6 nm)/sensing medium. Adding thin layers of ZnSe and black phosphorus to the Ag layer improved the biosensor sensitivity and resulted in a sharp dip in the resonance profile. The ZnSe layer above silver offers the necessary shielding and sensitivity increase since silver has a negative chemical interaction with the buffer solution.

After the effects of the different prisms of these sensors were analyzed, the CaF2/Ag/ZnSe/BP/SM-based sensor was characterized further, as it provided the highest sensitivity of 511 deg/RIU. The other parameters under optimum conditions obtained for this combination were a QF of 108.37751 (1/RIU), FoM of 108.374, FWHM of 4.715 (deg), and DA of 0.212089 (1/deg). This highly sensitive SPR biosensor design prevents unwanted pricking of the needle to extract blood samples from diabetic patients. Thus, the glucose level of diabetic patients can be determined through urine samples. The investigations performed in this research might also be added to future technical advances in glucose sensing, studies, and research. This design might have advantages in the fields of environmental, biomedical, and chemical studies, as well as virus detection, with new prospects.

Fig. 14 Fabrication steps for the proposed SPR sensor



Author Contribution Kazi Mustafizur Rahman– Conceptualization, Methodology, Visualization, Validation, Formal Analysis, Software, Writing – original draft, Investigation; Md. Faysal Nayan – Visualization, Validation, Formal Analysis, Writing – review & editing; Raihan Ahmed – Visualization, Formal Analysis; MD. Mushfiqur Rahman – Visualization, Formal Analysis. All the authors have read and approved the final version of the manuscript.

Data Availability No datasets were generated or analysed during the current study.

Declarations

Ethics Approval This study did not require ethics approval because it did not involve human participants, animal subjects, or other sensitive data.

Consent for Publication All the authors have given their consent to publish this work.

Competing Interest The authors declare no competing interests.

References

- Zayats AV, Smolyaninov II, Maradudin AA (2005) *Phys Rep* 408:131–314
- Pitarke JM, Silkin VM, Chulkov EV, Echenique PM (2007) *Rep Prog Phys* 70:1–87
- Abdulhalim I, Zourob M, Lakhtakia A (2008) *Electromagnetics (UK)* 28:214–242
- Kretschmann E, Raether H (1968) Notizen: radiative decay of non radiative surface plasmons excited by light. *Zeitschrift für Naturforschung A* 23(12):2135–2136. <https://doi.org/10.1515/zna-1968-1247>. [Online]. Available: doi:10.1515/zna-1968-1247
- Otto A (1968) Excitation of nonradiative surface plasma waves in silver by the method of frustrated total reflection. *Zeitschrift für Physik A Hadrons nuclei* 216(4):398–410
- Gupta S, Ramesh K, Ahmed S, Kakkar V (2016) Lab-on-chip technology: a review on design trends and future scope in biomedical applications. *Int J Bio-Sci Bio-Technol* 8(5):311–322
- Kumar S, Yadav A, Kumar S, Malomed BA (2024) Design and simulation of SPR sensors by employing silicon and silicon-nitride with mono and bimetal layers for sensitivity enhancement. *IEEE Sens J* 24(6):7671–7680. <https://doi.org/10.1109/jsen.2024.3355766>
- Szunerits S, Castel X, Boukherroub R (2008) Surface plasmon resonance investigation of silver and gold films coated with thin indium tin oxide layers: influence on stability and sensitivity. *J Phys Chem C* 112(40):15813–15817
- Zhang Q, Li H, Ma Y, Zhai T (2016) ZnSe nanostructures: synthesis, properties and applications. *Progress in Materials Science/Progress in Materials Science* 83:472–535. <https://doi.org/10.1016/j.pmatsci.2016.07.005>. Available: doi:10.1016/j.pmatsci.2016.07.005
- Chu Q, Han B, Jin Y, Guo S, Jin S, Park E, Chen L, Mee Jung Y (2020) Surface plasmon resonance induced charge transfer effect on the Ag-ZnSe-PATP system. *Spectrochimica Acta A Mol Biomol Spectrosc*. Epub 2020 Nov 16. PMID: 33257248
- Maheswari P, Subanya S, Ravi V, Rajesh KB, RajanJha JZ (2022) Platinum layers sandwiched between black phosphorous and graphene for enhanced SPR sensor performance. *Plasmonics* 17:213–222
- Mao N, Tang J, Xie L, Juanxia Wu, Han B, Lin J, Deng S, Ji W, HuaXu KL, Tong L, Zhang J (2016) Optical anisotropy of black phosphorus in the visible regime. *J Am Chem Soc* 138:300–305
- Srivastava T, Jha R (2018) Black phosphorus: a new platform for gaseous sensing based on surface plasmon resonance. *IEEE* 30:319–322
- Neethirajan S, Ragavan V, Weng X, Chand R (2018) Biosensors for sustainable food engineering: challenges and perspectives. *Biosensors* 8(1):23. <https://doi.org/10.3390/bios8010023>
- Hu C, Gan N, Chen Y, Bi L, Zhang X, Song L (2009) Detection of microcystins in environmental samples using surface plasmon resonance biosensor. *Talanta* 80(1):407–410. <https://doi.org/10.1016/j.talanta.2009.06.044>
- Sathya N, Karki B, Rane K et al (2022) Tuning and sensitivity improvement of bi-metallic structure-based surface plasmon resonance biosensor with 2-D ε-tin selenide nanosheets. *Plasmonics* 17:1001–1008. <https://doi.org/10.1007/s11468-021-01565-9>
- Almawgani AHM, Daher MG, Taya SA et al (2022) Detection of blood plasma concentration theoretically using SPR-based biosensor employing black phosphor layers and different metals. *Plasmonics* 17:1751–1764. <https://doi.org/10.1007/s11468-022-01662-3>
- Almawgani AHM, Daher MG, Taya SA, Mashagbeh M, Colak I (2022) Optical detection of fat concentration in milk using MXene-based surface plasmon resonance structure. *Biosensors* 12(7):535. <https://doi.org/10.3390/bios12070535>. Available: doi:10.3390/bios12070535
- Daher MG, Trabelsi Y, Ahmed NM et al (2022) Detection of basal cancer cells using photodetector based on a novel surface plasmon resonance nanostructure employing perovskite layer with an ultra high sensitivity. *Plasmonics* 17:2365–2373. <https://doi.org/10.1007/s11468-022-01727-3>
- Daher MG, Trabelsi Y, Prajapati YK et al (2023) Highly sensitive detection of infected red blood cells (IRBCs) with plasmodium falciparum using surface plasmon resonance (SPR) nanostructure. *Opt Quant Electron* 55:199. <https://doi.org/10.1007/s11082-022-04466-1>
- Daher MG (2023) Supersensitive biosensor based on a photonic crystal nanostructure for blood sugar level monitoring with ultra-high quality factor and low detection limit. *Optik* 275:170581. <https://doi.org/10.1016/j.ijleo.2023.170581>
- Mudgal N, Saharia A, Agarwal A, Ali J, Yupapin P, Singh G (2020) Modeling of highly sensitive surface plasmon resonance (SPR) sensor for urine glucose detection. *Opt Quantum Electron* 52(6):1–14. <https://doi.org/10.1007/s11082-020-02427-0>
- Mostufa S, Paul AK, Chakrabarti K (2021) Detection of hemoglobin in blood and urine glucose level samples using a graphene-coated SPR based biosensor. *OSA Continuum* 4(8):2164. <https://doi.org/10.1364/osac.433633>. [Online]. Available: doi:10.1364/osac.433633
- Karim MN, Anderson SR, Singh S, Ramanathan R, Bansal V (2018) Nanostructured silver fabric as a free standing NanoZyme for colorimetric detection of glucose in urine. *Biosens Bioelectron* 110:8–15. <https://doi.org/10.1016/j.bios.2018.03.025>
- Sani MH, Khosroabadi S (2020) A novel design and analysis of high-sensitivity biosensor based on nanocavity for detection of blood component, diabetes, cancer and glucose concentration. *IEEE Sens J* 20(13):7161–7168. <https://doi.org/10.1109/JSEN.2020.2964114>
- Singh S, Sharma AK, Lohia P et al (2022) Design and modeling of high-performance surface plasmon resonance refractive index sensor using BaTiO₃. MXene and nickel hybrid nanostructure *Plasmonics* 17:2049–2062. <https://doi.org/10.1007/s11468-022-01692-x>

27. Singh S, Pandey S, Yadav S et al (2024) Numerical study among Au, Al, and Ag metal-based surface plasmon resonance sensor. *J Opt* 53:304–314. <https://doi.org/10.1007/s12596-023-01107-y>
28. Karki B, Ansari G, Uniyal A et al (2023) PtSe₂ and black phosphorus employed for sensitivity improvement in the surface plasmon resonance sensor. *J Comput Electron* 22:106–115. <https://doi.org/10.1007/s10825-022-01975-w>
29. Srivastava A, Prajapati YK (2022) Surface plasmon resonance (SPR)-based biosensor using MXene as a BRE layer and magnesium oxide (MgO) as an adhesion layer. *J Mater Sci: Mater Electron* 33:8519–8528. <https://doi.org/10.1007/s10854-021-06436-x>
30. Brahmachari K, Ray M (2013) Effect of prism material on design of surface plasmon resonance sensor by admittance loci method. *Front Optoelectron* 6(2):185–193
31. El-assar M, Taha TE, El-Samie FEA et al (2023) ZnSe-based highly sensitive SPR biosensor for detection of different cancer cells and urine glucose levels. *Opt Quant Electron* 55:76. <https://doi.org/10.1007/s11082-022-04326-y>
32. Monzón-Hernández D, Velázquez-González JS, Luna-Moreno D, Torres-Cisneros M, Hernán dez-Roma I (2018) Prism-based surface plasmon resonance for dual-parameter sensing. *IEEE Sens* 18(10):4030–4037
33. Marple DTF (1964) Refractive index of ZnSe, ZnTe, and CdTe. *J Appl Phys* 35:539–542
34. Yesudasu V, Pradhan HS, Pandya RJ et al (2024) Numerical investigation of Ag-Franckeite-barium titanium-BP-based highly performed surface plasmon resonance sensor for virus SARS-CoV-2 detection. *Plasmonics* 19:167–178. <https://doi.org/10.1007/s11468-023-01985-9>
35. Karki B, Ramya KC, Sandhya Devi RS et al (2022) Titanium dioxide, black phosphorus and bimetallic layer-based surface plasmon biosensor for formalin detection: numerical analysis. *Opt Quant Electron* 54:451. <https://doi.org/10.1007/s11082-022-03875-6>
36. Chen WP, Chen JM (1981) Use of surface plasma waves for determination of the thickness and optical constants of thin metallic films. *J Opt Soc Am* 71(2):189. <https://doi.org/10.1364/josa.71.000189>. [Online]. Available: [doi:10.1364/josa.71.000189](https://doi.org/10.1364/josa.71.000189)
37. Katsidis CC, Siapkias DI (2002) General transfer-matrix method for optical multilayer systems with coherent, partially coherent, and incoherent interference. *Appl Opt* 41(19):3978. <https://doi.org/10.1364/ao.41.003978>. [Online]. Available: [doi:10.1364/ao.41.003978](https://doi.org/10.1364/ao.41.003978)
38. Yuan Y, Ding L, Guo Z (2011) Numerical investigation for SPR-based optical fiber sensor. *Sens Actuators, B Chem* 157(1):240–245. <https://doi.org/10.1016/j.snb.2011.03.056>. [Online]. Available: [doi:10.1016/j.snb.2011.03.056](https://doi.org/10.1016/j.snb.2011.03.056)
39. Fouad S, Sabri N, Poopalan P, Jamal ZAZ (2017) Surface plasmon resonance sensor sensitivity enhancement using gold- dielectric material. *Int J Nanoelectron Mater* 10:147–156
40. Mohanty G, Akhtar J, Sahoo BK (2016) Effect of semiconductor on sensitivity of a graphene-based surface plasmon resonance biosensor. *Plasmonics* 11(1):189–196. <https://doi.org/10.1007/s11468-015-0033-0>
41. Pandey AK, Sharma AK, Marques C (2020) On the application of SiO₂/SiC grating on Ag for high-performance fiber optic plasmonic sensing of cortisol concentration. *Materials* 13(7):1–13
42. Sharma P, Sharan P (2015) Design of photonic crystal-based biosensor for detection of glucose concentration in urine. *IEEE Sens J* 15(2):1035–1042. <https://doi.org/10.1109/JSEN.2014.2359799>
43. Karki B, Jha A, Pal A, Srivastava V (2022) Sensitivity enhancement of refractive index-based surface plasmon resonance sensor for glucose detection. *Optic Quant Electron* 54(9). <https://doi.org/10.1007/s11082-022-04004-z>
44. Mudgal N, Saharia A, Agarwal A, Singh G (2020) ZnO and Bimetallic (Ag–Au) layers based surface plasmon resonance (SPR) biosensor with BaTiO₃ and graphene for biosensing applications. *IETE J Res*. <https://doi.org/10.1080/03772063.2020.1844074>
45. Daher MG, Trabelsi Y, Ahmed NM et al (2023) Detection of *Escherichia coli* using highly sensitive surface plasmon resonance nanostructure (SPRN) based on MXene 2D nanomaterial. *Plasmonics* 18:2483–2492. <https://doi.org/10.1007/s11468-023-01970-2>
46. Kushwaha AS, Kumar A, Kumar R, Srivastava SK (2018) A study of surface plasmon resonance (SPR) based biosensor with improved sensitivity. *Photonics Nanostruct-Fundam Appl* 31(June):99–106. <https://doi.org/10.1016/j.photonics.2018.06.003>
47. Daher MG, Taya SA, Almawgani AHM et al (2023) Optical biosensor based on surface plasmon resonance nanostructure for the detection of mycobacterium tuberculosis bacteria with ultra-high efficiency and detection accuracy. *Plasmonics* 18:2195–2204. <https://doi.org/10.1007/s11468-023-01938-2>
48. Daher MG, Ahmed NM, Als Salman O et al (2023) Novel efficient surface plasmon resonance biosensor for the determination of sucrose concentration. *Plasmonics* 18:2069–2075. <https://doi.org/10.1007/s11468-023-01928-4>
49. Luna-Moreno D, Sánchez-álvarez A, Rodríguez-Delgado M (2020) Optical thickness monitoring as a strategic element for the development of SPR sensing applications. *Sensors (switzerland)*. <https://doi.org/10.3390/s20071807>
50. Smith JB, Hagaman D, Ji HF (2016) Growth of 2D black phosphorus film from chemical vapor deposition. *Nanotechnology* 27(21):1–8. <https://doi.org/10.1088/0957-4484/27/21/215602>

Publisher's Note Springer Nature remains neutral with regard to jurisdictional claims in published maps and institutional affiliations.

Springer Nature or its licensor (e.g. a society or other partner) holds exclusive rights to this article under a publishing agreement with the author(s) or other rightsholder(s); author self-archiving of the accepted manuscript version of this article is solely governed by the terms of such publishing agreement and applicable law.